analytical chemistry

ARTICLE

pubs.acs.org/ac

Slow-Equilibration Approximation in Macroscopic Approach to Studying Kinetics at Equilibrium

Leonid T. Cherney and Sergey N. Krylov*

Department of Chemistry and Centre for Research on Biomolecular Interactions, York University, Toronto, Ontario M3J 1P3, Canada

ABSTRACT: Macroscopic approach to studying kinetics at equilibrium (MASKE) facilitates measurements of rate constants of formation (k_+) and dissociation (k_-) of affinity complexes in the state of chemical equilibrium. MASKE relies on "informational nonequilibrium" created by a nonuniform initial spatial distribution of a label on one of the reactants. In general, finding k_+ and k_- by MASKE requires fitting experimental label-propagation patterns—dependencies of label concentrations on a coordinate or time—with the simulated label-propagation patterns. Here we introduce a simple fitting-free approach for finding the rate constants in the case of slow equilibration. Slow equilibration means that the characteristic equilibration time of the labeled reactant and labeled complex, t_{eq}, is much greater than the characteristic separation time of the labeled reactant and labeled complex, t_{sep}. We developed the mathematics for this approach by solving the differential equations of mass transfer using the assumption of slow equilibration. The approach was then tested and its accuracy was studied by applying it to label-propagation patterns created with the earlier-developed exact solution of the mass-transfer equations. The results proved that the approximate solution was correct. They also showed that k_+ and k_- can be found with this fitting-free approach with a relative error less than 20% if $t_{sep} < 0.6t_{eq}$. The practical limitations of our slow-equilibration approximation are discussed.

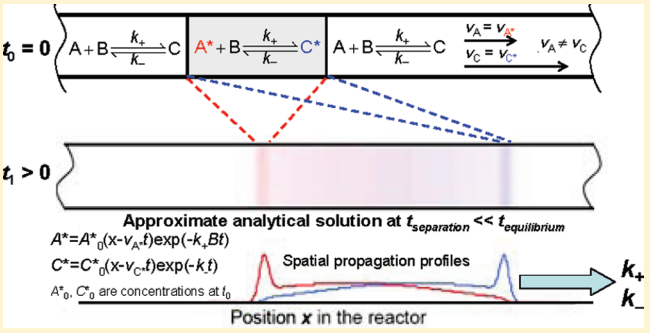

Affinity interactions are highly selective multibond interactions of biological molecules with a formation of stable noncovalent complexes.[1,2] Such interactions play a key role in regulation of cellular processes, for example, gene expression, DNA replications, signal transduction, etc.[3−7] Understanding the molecular mechanisms of these biological processes requires the knowledge of kinetics and thermodynamics of the involved affinity interactions. For the purpose of studying kinetics and thermodynamics, the binding of molecules A and B with a formation of complex C can be written as a simple chemical equation:

$$A + B \underset{k_-}{\overset{k_+}{\rightleftarrows}} C \qquad K_d = k_-/k_+ \qquad (1)$$

where k_+ and k_- are rate constants of complex formation and dissociation, respectively, and K_d is the equilibrium dissociation constant. The goal of kinetic and thermodynamic studies is essentially to find k_+, k_-, and K_d. Note that since the three constants are interlinked finding either two is sufficient for calculating a third one.

We recently introduced macroscopic approach to studying kinetics at equilibrium (MASKE) that allows finding k_+, k_-, and K_d in the state of chemical equilibrium.[8] The essence of MASKE is the following. First, two equilibrium mixtures, nonlabeled and labeled, are prepared by mixing B with nonlabeled A and labeled A (A*), respectively:

$$A + B \underset{k_-}{\overset{k_+}{\rightleftharpoons}} C \qquad (2)$$

$$A^* + B \underset{k_-}{\overset{k_+}{\rightleftharpoons}} C^* \qquad (3)$$

where * is a detectable label which does not significantly affect k_+ and k_-. Second, a one-dimensional (long and narrow) reactor is filled with the nonlabeled mixture along all its length except for a part, which is filled with the labeled mixture (Figure 1). Third, a differential mobility of A with respect to C is then introduced along the reactor in a way that the label does not significantly change the velocities of labeled A and C. The one-dimensional reactor is connected at its ends to two large reservoirs with the nonlabeled mixture to ensure there is a continuous supply of the reaction components in the reactor. The MASKE setup allows for the chemical equilibrium between A + A*, B, and C + C* to be maintained through the whole reactor length at all times. As a result of the equilibrium, concentrations of A + A*, B, and C + C* do not change with time or spatial coordinate. Label propagation through the reactor will depend on how fast A* and C* equilibrate with respect to the rate of their separation. The equilibration and separation processes for A* and C* are characterized by corresponding characteristic equilibration time,

Received: October 20, 2010
Accepted: January 2, 2011
Published: January 24, 2011

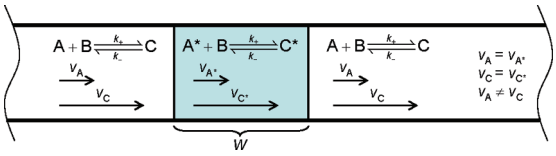

Figure 1. Schematic representation of the MASKE setup in its initial condition with a single zone of the labeled equilibrium mixture (blue) surrounded by the nonlabeled equilibrium mixture.

t_{eq}, and characteristic separation time, t_{sep}. The label-propagation pattern qualitatively depends on how the value of t_{eq} relates to that of t_{sep}. Finally, the values of k_+ and k_- are found from either a spatial or a temporal label-propagation pattern. The spatial pattern is a label concentration versus the coordinate at a fixed time. The temporal pattern is a label concentration versus time at a fixed coordinate.

All other methods of finding rate constants are based on studying kinetics under conditions when the chemical equilibrium is either perturbed or impossible due to the microscopic nature of a system.[9−15] Heterogeneous perturbed-equilibrium methods, such as surface plasmon resonance, utilize reactant A immobilized on a solid substrate and reactant B in solution contacting the surface.[9] The chemical equilibrium is perturbed by changing the solution in contact with the surface from that of B to the pure buffer or vise versa. Heterogeneous methods often suffer from nonspecific binding of B to the surface and from changes in the affinity between A and B caused by the immobilization. Homogeneous perturbed-equilibrium methods include several kinetic capillary electrophoresis methods that perturb the chemical equilibrium by means of manipulating concentration gradients of A, B, and C in solution through the introduction of their differential mobilities.[10−12] Concentration nonuniformity can result in molecules acquiring different conformations/structures in different parts of the reactor, for example, due to their aggregation. This may obscure the determination of k_+ and k_-. Besides, the analysis of chemical kinetics for homogeneous nonequilibrium reactions usually requires somewhat "nontransparent" numerical procedures.

Microscopic kinetic methods track concentration fluctuations in a volume sufficiently small for the equilibrium not to be attainable due to a small number of molecules in this volume. The examples of such methods are fluorescence correlation spectroscopy, nanopore amperometry, and some setups of fluorescence resonance energy transfer.[13−15] The small number of molecules makes impossible the use of informative detection methods such as mass spectrometry. Besides, "microscopic" methods are usually more complicated than macroscopic ones.

Two conceptually different approaches exist for "extracting" values of k_+ and k_- from the label-propagation patterns in MASKE. The first approach is "classical" pattern-based. In this approach, a simulated label-propagation pattern is built by solving differential equations of mass transfer for the label. The simulated pattern is then fitted into the experimental pattern through nonlinear regression by varying k_+ and k_- until the best fit is found. The values of k_+ and k_- that correspond to the best fit are considered to be the sought ones. The second approach is parameter-based; it relies on obtaining from the experimental label-propagation pattern a small number of numerical parameters that are then utilized to calculate k_+ and k_- using relatively simple algebraic equations. Label-propagation patterns in MASKE can be classified into three categories: (i) single zone of the label for fast equilibration ($t_{eq} \ll t_{sep}$), (ii) two separated zones of the label for slow equilibration ($t_{eq} \gg t_{sep}$), and (iii) two overlapping zones of the label for same-order equilibration and separation ($t_{eq} \sim t_{sep}$) (Figure 2, see also definitions 5 for t_{eq} and t_{sep}). We use a term "bridge" for the overlapping part of the zones. Numerical parameters, such as zone heights, zone widths, zone's travel time to a detector, and total label amounts in the zones can be used to characterize label-propagation patterns. In the original MASKE work, a parameter-based method for finding k_- and K_d was developed for the case of fast equilibration: $t_{eq} \ll t_{sep}$. It is based on measuring widths and travel time of the label zone as a function of concentration of B. The method was shown to be accurate in finding k_- and K_d to 10% even for a relatively weak inequality of $t_{eq} < 3t_{sep}$.

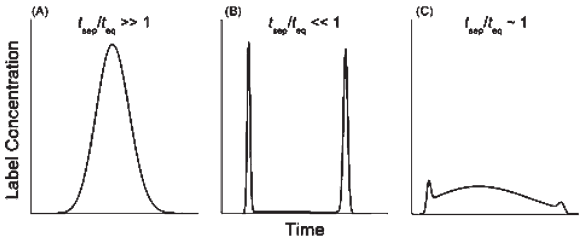

Figure 2. Three types of label-propagation patterns depending on ratios between the characteristic separation and equilibration times, t_{sep}/t_{eq}: (A) a single zone during all time, (B) two separate zones shortly after introducing an initial zone of the label, and (C) two overlapping zones.

The goal of this work was to develop a parameter-based method for finding k_+ and k_- in MASKE in case of slow equilibration. To achieve this, we solved differential equations of mass transfer for the label in the approximation of slow equilibration: $t_{eq} \gg t_{sep}$. The result was algebraic equations for k_+ and k_- which include only the parameters obtained from the temporal label-propagation patterns. These parameters are total label amounts, $A^*_{tot}(t)$ and $C^*_{tot}(t)$, or maximum label concentrations, $A^*_h(t)$ and $C^*_h(t)$, in the separated zones moving with migration velocities of compounds A* and C*, respectively. To obtain the required parameters, we propose an experimental design for MASKE with a single point detector (such as one in capillary electrophoresis). Two MASKE experiments should be performed under similar conditions with the only difference being the length of the reactor from the initial position of the labeled equilibrium mixture to the detector. We tested the proposed approach using simulated temporal propagation patterns obtained with the exact solution of MASKE equations.[8] The use of the simulated label-propagation patterns also allowed us to study the accuracy of the determination of k_+ and k_- by the slow-equilibration approximation. The results showed that the values of k_+ and k_- do not significantly differ (see Figure 4) from the real ones if $t_{sep} < 0.6t_{eq}$. The slow equilibration approximation of MASKE will be applicable to the interactions of larger biomolecules, which are often characterized by slow binding and slow dissociation. The next challenge in the development of simplified mathematics for MASKE will be the development of a parameter-based method for the intermediate case of $t_{eq} \sim t_{sep}$, when a considerable zone overlap is present.

RESULTS AND DISCUSSION

Approximate Solution of Mass-Transfer Equations. We consider the following theoretical setup of MASKE (see Figure 1).

A one-dimensional infinite reactor is coaxial with the x-coordinate. In such a reactor, in general, concentration gradients and mass transport are possible only along the x-axis (a long capillary is a practical example of such a reactor). A reversible binary reaction of a reactant A with a reactant B forming an affinity complex C, with rate constants of forward and reverse processes of k_+ and k_-, respectively, is in the state of chemical equilibrium. In MASKE, mass transfer of A* and C* is considered in case of negligible diffusion and described by the following equations:

$$\begin{aligned}(\partial_t + v_A\,\partial_x)A^* &= -k_+A^*B + k_-C^*\\ (\partial_t + v_C\,\partial_x)C^* &= k_+A^*B - k_-C^*\end{aligned} \quad (4)$$

where ∂_x and ∂_t are partial derivations by spatial coordinate and time, respectively; A^* and C^* can be considered as linear concentrations of A* and C*, respectively (i.e., amounts of A* and C* per unit length of the reactor); B is a volume concentration of B; and v_A and v_C are the velocities of A* and C*. In constraints of MASKE, A^* and C^* change with time and coordinate, whereas B = const no matter what the relation between B and A is.[8] B stays constant because MASKE assumes that migration velocities of A and B and the rate constants k_+ and k_- are not affected by the label. This assumption will usually be valid if the size of the label is much smaller than those of A and B. All obtained results will be valid in a more general case of B = const. The latter can be achieved, for example, when B is present in a large access to A and C. If B = const, the exact MASKE solution used below in error estimates will hold true. Furthermore, if B = const, basic eqs 4 and final expressions 11 and 13 for rate constants will not depend on the migration velocities of unlabeled A and C. Therefore, the methods developed below are valid regardless of whether or not the labeling affects the migration velocities of A and C as long as B remains constant. The requirement that labeling does not affect k_+ and k_- is still valid.

After introducing A* and C* in the reactor as an initial zone of spatial width W, the later spatial and temporal distributions of A* and C* are defined by two competing processes that are described by eqs 4. The first process is the movement of A* and C* with different velocities (we assume for definitiveness that $v_C > v_A > 0$) that results in their separation. The second process is the forward and reverse reactions 3 between A*, B, and C* that lead to equilibration between A* and C*. The characteristic times of separation and equilibration, t_{sep} and t_{eq}, respectively, are given by[8]

$$t_{sep} = \frac{W}{|v_C - v_A|}, \quad t_{eq} = \frac{1}{k_+B + k_-} \quad (5)$$

Here, we define t_{sep} using the full width W (along the capillary) of the initial zone rather than the half-width $W/2$ as in ref 8. Definition 5 for t_{sep} based on full width W corresponds to an upper estimate for t_{sep}. If the concentration profile in the initial zone is modeled by the Gaussian distribution, then W is defined as a distance between points where the total concentration of A* and C* is equal to 1% of its maximum value.

If $t_{sep} \ll t_{eq}$, an approximate solution of eqs 4 can be obtained. In this case, the characteristic times t_+ and t_- of the forward and reverse chemical reactions are much greater than the separation time:

$$\begin{aligned}t_+ &\equiv (k_+B)^{-1} > t_{eq} \gg t_{sep},\\ t_- &\equiv (k_-)^{-1} > t_{eq} \gg t_{sep}\end{aligned} \quad (6)$$

Therefore, the effect of the chemical reaction on a change in the concentrations A^* and C^* in eqs 4 is negligible at $t \sim t_{sep}$, and initial zones of A* and C* will be separated at $t \gg t_{sep}$. After the separation, C* can be present in the zone of A* only as a result of the forward reaction 3 for the labeled compounds. Similarly, A* can be present in the zone of C* only as a result of the reverse reaction 3 for the labeled compounds. However, products of such reactions are removed from the corresponding zones in a "short" time $t_{rem} \sim t_{sep}$, and therefore, $t_{rem} \ll t_+$ and $t_{rem} \ll t_-$. As a result, we have $C^* \ll A^*$ in the zone of A* and $A^* \ll C^*$ in the zone of C* at all times $t \gg t_{sep}$. Since C* is depleted in the zone of A*, the term k_-C^* in the first eq 4 is small and can be omitted. However, we must keep the term $-k_+A^*B$ in the first eq 4 at $t \gg t_{sep}$ since in this case t may be comparable with the characteristic time t_+ of the forward reaction, and A* is obviously not depleted in the zone of A*. Similarly, A* is depleted in the zone of C* and we can omit the term k_+A^*B in the second eq 4 but we must keep the term k_-C^* in this equation at $t \gg t_{sep}$. After such simplifications, eqs 4 can be readily solved. They give the following distributions of A^* and C^* in the zones of A* and C*, respectively:

$$\begin{aligned}A^* &= a^*(x - v_At)\exp(-k_+Bt),\\ C^* &= c^*(x - v_Ct)\exp(-k_-t)\end{aligned} \quad (7)$$

Here, $a^*(x)$ and $c^*(x)$ are distributions of concentrations A^* and C^* in the initial zone of the labeled equilibrium mixture at $t = 0$. Note that expressions 7 can also be derived directly from the general solution of MASKE that was obtained previously in the Supporting Information for ref 8. It is obvious from expressions 7 that the zones of A* and C* move with velocities v_A and v_C, respectively. The widths of these zones have the order of W, and expressions 7 become not valid near the boundaries of the zones. The total amounts of the compounds A* and C*

$$A^*_{tot} = \int A^*\,dx, \quad C^*_{tot} = \int C^*\,dx \quad (8)$$

in these zones are exponentially decreasing with time:

$$\begin{aligned}A^*_{tot} &= a^*_{tot}\exp(-k_+Bt),\\ C^*_{tot} &= c^*_{tot}\exp(-k_-t)\end{aligned} \quad (9)$$

Here, a^*_{tot} and c^*_{tot} are total amounts of the corresponding compounds in the initial zone at $t = 0$. They are defined by relations

$$a^*_{tot} = \int a^*\,dx, \quad c^*_{tot} = \int c^*\,dx \quad (10)$$

Relations 9 and 10 allow the rate constants of the forward and reverse reaction 1 to be determined in a parameter-based approach if total amounts of compounds A^*_{tot} and C^*_{tot} in the zones of A* and C* are measured at some time $t > 0$. Importantly, this can be done even if the total amounts of compounds a^*_{tot} and c^*_{tot} in the initial zone are unknown. In this case, one should find values of A^*_{tot} at two different times t_{A1} and t_{A2} and also find values of C^*_{tot} at two (other) times t_{C1} and t_{C2} (Figure 3). The substitution of these data in eq 9 leads to a system of simple equations that yield the following expressions for the rate constants of reaction 1:

$$\begin{aligned}k_+ &= \frac{1}{B(t_{A2} - t_{A1})}\ln\frac{A^*_{tot}(t_{A1})}{A^*_{tot}(t_{A2})},\\ k_- &= \frac{1}{t_{C2} - t_{C1}}\ln\frac{C^*_{tot}(t_{C1})}{C^*_{tot}(t_{C2})}\end{aligned} \quad (11)$$

An alternative method of finding k_+ and k_- can be based on measuring the heights of peaks, A^*_h and C^*_h, at two different

dx.doi.org/10.1021/ac102768r |Anal. Chem. 2011, 83, 1381–1387

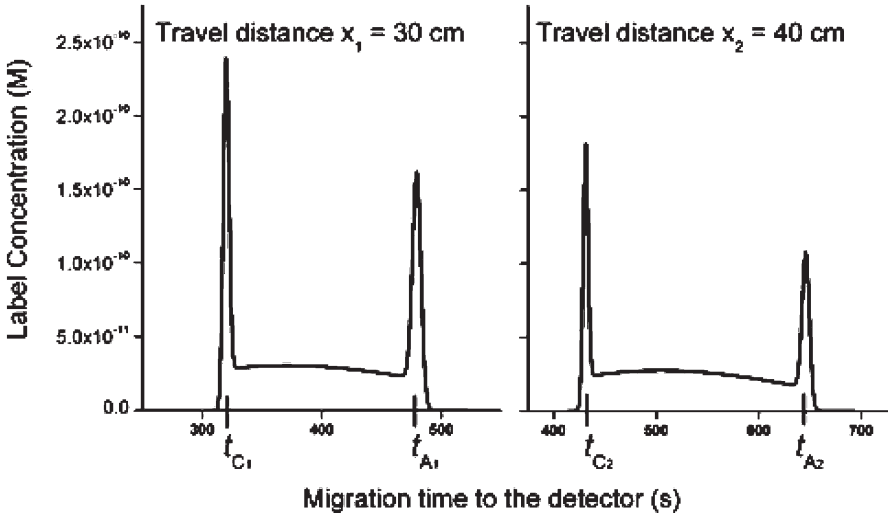

Figure 3. Examples of simulated temporal label-propagation patterns in the presence of noise (2% of the background). Peaks appear at different times for different travel distances x_1 and x_2 from the initial label zone to a detector. With increasing time, the peak heights and areas decrease, and the distance between the peaks increases.

times rather than the areas of peaks (the peak heights correspond to maximum concentrations of corresponding components in their zones). Indeed, relations 7 yield the following dependencies of the peak heights on time:

$$A^*_h = a^*_h \exp(-k_+ Bt), \quad C^*_h = c^*_h \exp(-k_- t) \quad (12)$$

where a^*_h and c^*_h are the heights of the initial peaks of A* and C* (maximum concentrations in the initial zone). Substitution of A^*_h and C^*_h measured at t_{A1}, t_{A2} and t_{C1}, t_{C2}, respectively (Figure 3), transforms eq 12 into a system of equations that can be readily solved with respect to k_+ and k_-. As a result, we obtain expressions that are similar to eq 11:

$$k_+ = \frac{1}{B(t_{A2} - t_{A1})} \ln \frac{A^*_h(t_{A1})}{A^*_h(t_{A2})},$$

$$k_- = \frac{1}{t_{C2} - t_{C1}} \ln \frac{C^*_h(t_{C1})}{C^*_h(t_{C2})} \quad (13)$$

The method of finding k_+ and k_- based on the peak heights allows the verification of the k_+ and k_- values determined from the peak areas. This method can also be useful if the peak areas are poorly defined (due to uncertainty in boundary positions) and do not produce reliable values of k_+ and k_-. However, finding k_+ and k_- from the peak heights depends entirely on measurements at only a few specific moments of time corresponding to the peak heights. In general, such a method is more prone to errors than the one based on peak areas.

Relations between Concentrations and Signals. All above equations use concentrations or total amount of compound A* and C*, whereas the experimental traces of MASKE, such as electropherograms, operate with a signal (optical, electrochemical, etc.). It is instructive to consider the relations between the concentrations and signals using an example of fluorescence detection. If fluorescence detection is used with a detector placed at some point x^{det}, temporal dependencies of A^* and C^* at that point are related to fluorescence signals A_f and C_f in the following way:

$$A^*(x^{det}, t) = \chi_A \frac{A_f(x^{det}, t)}{t_A Q_A},$$

$$C^*(x^{det}, t) = \chi_C \frac{C_f(x^{det}, t)}{t_C Q_C} \quad (14)$$

Here χ_A and χ_C are the proportionality coefficients, which depend on fluorophores and detectors used for A* and C*, t_A and t_C are residence times of A* and C* in the detectors, Q_A and Q_C are absolute quantum yields of A* and C*. In a typical case, a single fluorophore and a single detector are used for both A* and C* resulting in $\chi_A = \chi_C = \chi$. It is worth noting that the ratio of the residence times is much easier to determine than individual residence times since

$$t_A/t_C = v_C/v_A = t_{MA}/t_{MC} \quad (15)$$

where t_{MA} and t_{MC} are migration times of the peaks of A* and C*, respectively, to the detector. The latter ratio is easily measured. Taking into account eq 15, we can present relations 14 in a more practical form:

$$A^*(x^{det}, t) = \alpha A_f(x^{det}, t),$$

$$C^*(x^{det}, t) = \frac{\alpha t_{MA}}{\varphi t_{MC}} C_f(x^{det}, t) \quad (16)$$

Here $\alpha = \chi/t_A Q_A$ can be treated as a calibration coefficient identical for both A* and C*, and $\varphi = Q_C/Q_A$ is a relative quantum yield that is measured much easier than absolute quantum yields.[16,17] It should also be noted that the heights of peaks of concentrations A^* and C^* are practically equal to the heights of peaks of the total label in zones of A* and C*, respectively, since $C^* \ll A^*$ in the zone of A* and $A^* \ll C^*$ in the zone of C*. As a result, values of A^*_h and C^*_h that appear in eq 13 can be determined based on fluorescence signals $(A + C)_f$ of the sum of A* and C*:

$$A^*_h(t_{Aj}) = \alpha(A + C)_f(x^{det}, t_{Aj}) \quad \text{at}$$

$$t_{Aj} = \frac{x^{det}_j}{v_A}, \quad j = 1, 2 \quad (17)$$

dx.doi.org/10.1021/ac102768r |Anal. Chem. 2011, 83, 1381–1387

$$C^*_h(t_{Cj}) = \frac{\alpha t_{MA}}{\varphi t_{MC}} (A+C)_f(x^{det}, t_{Cj}) \quad \text{at}$$

$$t_{Cj} = \frac{x_j^{det}}{v_C}, \quad j = 1,2 \tag{18}$$

Obviously, the concentrations of A* and C* in the reactor can be determined accurately based on fluorescence signals only if those concentrations do not change significantly by reactions 3 while the compounds remain in the detector. Hence, we assume that

$$k_+ B t_A \ll 1, \quad k_- t_C \ll 1 \tag{19}$$

and therefore the exponential functions in eq 7 do not change significantly during residence times of A* and C* in the detector.

In this case, the total amounts of A* and C* that appear in eq 11 are related to fluorescence signals in the following way:

$$A^*_{tot}(t_{Aj}) = v_A \alpha \int A_f(x_j^{det}, t)\, dt \quad \text{at}$$

$$t_{Aj} = \frac{x_j^{det}}{v_A}, \quad j = 1,2 \tag{20}$$

$$C^*_{tot}(t_{Cj}) = \frac{v_C \alpha t_{MA}}{\varphi t_{MC}} \int C_f(x_j^{det}, t)\, dt \quad \text{at}$$

$$t_{Cj} = \frac{x_j^{det}}{v_C}, \quad j = 1,2 \tag{21}$$

Here x_1^{det} and x_2^{det} are spatial coordinates of two different positions of the detector; t_{A1} and t_{A2} are time intervals that are required for the concentration peak of A* to reach the detector positions; similarly, t_{C1} and t_{C2} are time intervals that are required for the concentration peak of C* to reach the detector positions. We assume that A* and C* are introduced at $x = 0$. Integrals on the right-hand sides of eqs 20 and 21 represent areas of peaks of measurable signals. Again, values of A^*_{tot} and C^*_{tot} are practically equal to total label amounts in the corresponding zones since in each zone only the compound after which the zone is named is not depleted. As a result, A^*_{tot} and C^*_{tot} can be determined directly from the experimental MASKE trace corresponding to the sum of A* and C* meaning that integrands in eqs 20 and 21 can be replaced with values of the sum $(A + C)_f$ that represent measurable signals.

Generally speaking parameters α, φ, and t_{MA}/t_{MC} that appear in eqs 17, 18, 20, and 21 can affect expressions 11 and 13 for k_+ and k_-. However, these expressions depend on parameters α, φ, and t_{MA}/t_{MC} only through the ratios α_1/α_2, φ_1/φ_2, and $(t_{MA}/t_{MC})_1/(t_{MA}/t_{MC})_2$ where subscripts 1 and 2 are assigned to the corresponding values of the parameters for two different positions of the detector. If the values of parameters α, φ, and t_{MA}/t_{MC} for the two positions are identical, which is typically true, all above ratios become equal to 1. In this case, parameters α, φ, and t_{MA}/t_{MC} do not affect expressions for k_+ and k_-.

Test of Applicability of the Approximation Method of Rate Constants Determination. To study accuracy of finding k_+ and k_- based on expressions 11 and 13 derived from the approximate solution 7 we need temporal label-propagation patterns for various known values of k_+ and k_-. The best way to produce such patterns is to simulate them using the exact MASKE solution for eqs 4.[8] We have developed a program that allows one to change basic parameters (k_+, k_-, v_A, v_C, B, and W) and to add noise to the simulated electropherograms. Then such simulated electropherograms can be used to back-calculate k_+ and k_- based on expressions 11 or 13. Since the true values of k_+ and k_- are known in this case, corresponding relative errors δ_+ and δ_- (an absolute value of the ratio between the deviation from the true value and the true value) are easy to determine. The results are presented in Figure 4 that shows dependencies of δ_+ and δ_- on the dimensionless parameter t_{sep}/t_{eq} for two alternative methods of calculation of k_+ and k_- using peak areas and peak heights.

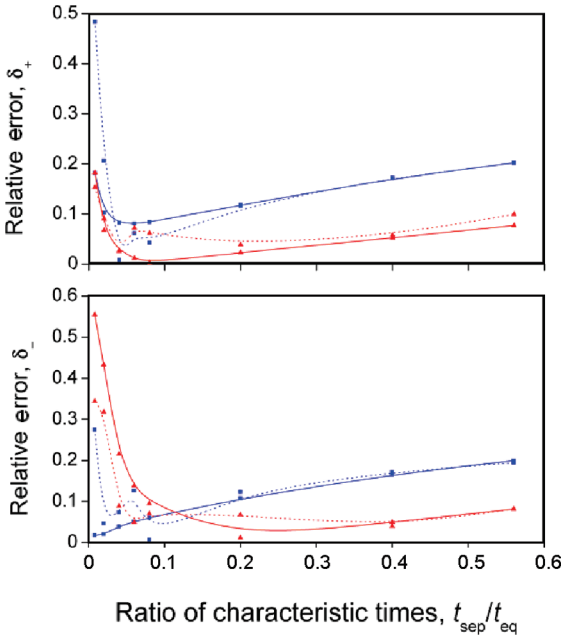

Figure 4. Relative errors δ_+ and δ_- in the determination of k_+ and k_-. Blue lines and red lines correspond to methods based on relations 11 for peak areas and 13 for peak heights, respectively. Simulation without noise is shown by the solid lines, whereas simulation with an added noise is depicted by the broken lines.

The following examples of simulation include values of k_+ and k_- typical for biomolecular interactions and reactor length typical for separation methods.[8] For a reactor length of 30−40 cm, the methods give the best results in an interval of t_{sep}/t_{eq} values that is presented in Figure 4. This fact can be explained as follows. The smallest value of $t_{sep}/t_{eq} = 0.008$ is achieved, for example, at $Bk_+ = k_- = 10^{-4}$ s^{-1}, $W = 1.2$ cm and $v_C - v_A = 0.03$ cm/s. In this case, the arguments of the exponential functions in eq 7 are of the order of 10^{-2} for a 30−40 cm long reactor and $v_C \sim 0.1$ cm/s. A further decrease in t_{sep}/t_{eq}, let's say, to 10^{-3}, at the same W will correspond to a decrease in k_+ and k_- (or to an increase in v_C and v_A) and will lead to values of those arguments of the order of 10^{-3}. As a result, changes in the peaks will become too small to detect them in a 30−40 cm long reactor without a significant increase in errors. In this case, calculation of k_+ and k_- based on eq 11 or eq 13 will require the use of a longer reactor. To study reactions with smaller values of k_+ and k_- one can also decrease v_C and v_A. The decrease will allow keeping the value of t_{sep}/t_{eq} in the interval shown in Figure 4.

An opposite situation with the peaks (too big changes) takes place for larger values of t_{sep}/t_{eq} within the interval of t_{sep}/t_{eq} presented in Figure 4. For example, a value of $t_{sep}/t_{eq} = 0.6$ is

achieved at $Bk_+ = k_- = 10^{-2}$ s^{-1}, $W = 1.2$ cm and $v_C - v_A = 0.04$ cm/s. In this case, the arguments of the exponential functions in eq 7 are of the order of 1 for a 30−40 cm long reactor and $v_C \sim 0.1$ cm/s. As a result, the heights of the peaks become comparable with the bridge height and even smaller than the latter (as demonstrated in Figure 2C). This makes calculations of the peak areas ambiguous and prone to large errors. (Interestingly, finding k_+ and k_- based on measurements of the peak heights remain possible with errors ~10% until the peaks disappear.) In this case, a shorter reactor should be used to determine k_+ and k_- based on eq 11 or eq 13, which, in turn, will require a decrease in the spatial width W of the initial zone. To study reactions with $Bk_+ > 10^{-2}$ s^{-1} and $k_- > 10^{-2}$ s^{-1}, one can also increase v_C and v_A so that the values of t_{sep}/t_{eq} remain in the interval presented in Figure 4.

Using these examples we can estimate the effect of diffusion that was neglected in basic eqs 4. The increase in the peak width δW due to diffusion is determined by the following relations:[18]

$$\delta W = \sqrt{D\tau} = \sqrt{DL/v} \qquad (\tau \equiv L/v) \qquad (22)$$

where D is the diffusion coefficient, τ is the characteristic time required for a peak to reach the detector, L is the distance from the injection end to the detector, v is the velocity of peak propagation. The diffusion coefficient can be estimated for large biomolecules (e.g., proteins, oligonucleotides) as $D \sim 10^{-6}$ cm^2/s.[19,20] Diffusion is negligible if

$$\frac{\delta W}{W} = \frac{L}{W\sqrt{Pe}} \ll 1 \qquad \left(Pe \equiv \frac{vL}{D}\right) \qquad (23)$$

were Pe is the Péclet number. We have $Pe \sim 10^6$ and $\delta W/W \sim 10^{-2}$ at $v \sim 0.1$ cm/s, $W \sim 1$ cm, and $L \sim 30$ cm. Therefore, the contribution of diffusion into δ_+ and δ_- is relatively small (~1%).

Though the interval of t_{sep}/t_{eq} shown in Figure 4 may seem to be small (0.008 ÷ 0.6), the corresponding intervals of k_+ and k_- can be significantly larger. The reason for this is that t_{sep}/t_{eq} depends not only on k_+ and k_- but also on v_C, v_A, and W. By changing the latter parameters one can apply the developed method to larger intervals of k_+ and k_- while keeping t_{sep}/t_{eq} within the limits shown in Figure 4. For example, the 10-fold decrease of v_C and v_A at the lower end of the t_{sep}/t_{eq} interval (as mentioned above) would allow the determination of Bk_+ and k_- within an interval of $10^{-5} \div 10^{-2}$ s^{-1}. The subsequent 10-fold increase of v_C and v_A at the upper end of the t_{sep}/t_{eq} interval would result in further expansion of intervals of Bk_+ and k_- up to $10^{-5} \div 10^{-1}$ s^{-1}. Besides, the interval of t_{sep}/t_{eq} shown in Figure 4 can be expanded by using longer and/or shorter capillary reactors.

It would be useful to study the effect of the choice of peak boundaries on relative errors δ_+ and δ_- found from calculations of the peak areas. In the simplest case, the peak widths could be defined as the initial zone width W rather than determined from the analysis of peak shape. As a result, the widths of both peaks will remain constant, whereas the peak heights A^*_h and C^*_h decrease at variable rates $-Bk_+A^*_h$ and $-k_-C^*_h$, respectively, that depend on the values of the peak heights. To study the pure effect of the peak boundaries, the simulation without noise is preferable. Figure 5 shows the effect of inaccuracy in the determination of peak boundaries caused by the rough estimate of the peak width being W or $2W$. Such an estimate affects δ_+ more than δ_- though the order of magnitude of both δ_+ and δ_- does not change. The peak boundaries should not include significant portions of the bridge as it would result in a large increase of both δ_+ and δ_-.

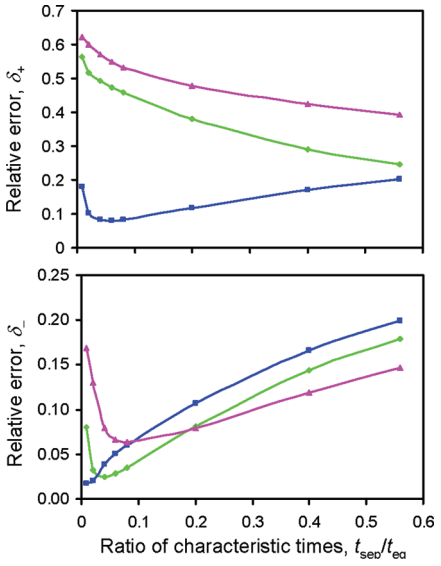

Figure 5. Relative errors δ_+ and δ_- for the method based on the peak areas if the peak widths equal to W (magenta lines) and $2W$ (green lines). Blue lines depict the same δ_+ and δ_- as in Figure 4.

CONCLUDING REMARKS

In this work, we introduced the second parameter-based method of finding k_+ and k_- in MASKE which works under the approximation of slow equilibration: $t_{sep}/t_{eq} \ll 1$. The parameters used in the method are (i) areas or heights of the peaks of A* and C* which migrate with velocities v_A and v_C, respectively, and (ii) travel times of the peaks to the detector. To exclude the need to know the initial distribution of A* and C* in the reactor, we suggest the use of reactors of two different lengths. The latter will make the method applicable to practical separation techniques, such as capillary electrophoresis. We tested the accuracy of the method by applying it to label-propagation patterns simulated with exact solution of MASKE equations.[8] We found that the method's accuracy was better than 20% for $t_{sep}/t_{eq} < 0.6$ except for very small values of Bk_+ and k_- of the order of 10^{-4} s^{-1}. This result was also a useful cross-validation of the method presented here and the exact solution of MASKE. We foresee that this uncomplicated method will be attractive to MASKE users due to its directness.

AUTHOR INFORMATION

Corresponding Author

*E-mail: skrylov@yorku.ca.

ACKNOWLEDGMENT

This work was funded by the Natural Sciences and Engineering Research Council of Canada.

REFERENCES

(1) George, A.; Gallop, J.; Rashid, M. *Expert Opin. Ther. Pat.* **1997**, *7*, 947–963.
(2) Muller-Dethlefs, K.; Hobza, P. *Chem. Rev.* **2000**, *100*, 143–167.
(3) Bell, S.; Dutta, A. *Annu. Rev. Biochem.* **2002**, *71*, 333–374.
(4) Kohn, K. *Mol. Biol. Cell* **1999**, *10*, 2703–2734.

(5) Nooren, I.; Thornton, J. *EMBO J.* **2003**, *22*, 3486–3492.
(6) Ullrich, A.; Schlessinger, J. *Cell* **1990**, *61*, 203–212.
(7) Vonhippel, P.; Bear, D.; Morgan, W.; McSwiggen, J. *Annu. Rev. Biochem.* **1984**, *53*, 389–446.
(8) Okhonin, V.; Berezovski, M. V.; Krylov, S. N. *J. Am. Chem. Soc.* **2010**, *132*, 7062–7068.
(9) Wilson, W. D. *Science* **2002**, *295*, 2103–2105.
(10) Berezovski, M.; Krylov, S. N. *J. Am. Chem. Soc.* **2002**, *124*, 13674–13675.
(11) Okhonin, V.; Krylova, S. M.; Krylov, S. N. *Anal. Chem.* **2004**, *76*, 1507–1512.
(12) Petrov, A.; Okhonin, V.; Berezovski, M.; Krylov, S. N. *J. Am. Chem. Soc.* **2005**, *127*, 17104–17110.
(13) Al-Soufi, W.; Reija, B.; Novo, M.; Felekyan, S.; Kuhnemuth, R.; Seidel, C. A. M. *J. Am. Chem. Soc.* **2005**, *127*, 8775–8784.
(14) Hornblower, B.; Coombs, A.; Whitaker, R. D.; Kolomeisky, A.; Picone, S. J.; Meller, A.; Akeson, M. *Nat. Methods* **2007**, *4*, 315–317.
(15) Li, Y.; Augustine, G. J.; Weninger, K. *Biophys. J.* **2007**, *93*, 2178–2187.
(16) Chartier, A.; Georges, J.; Mermet, J. *Chem. Phys. Lett.* **1990**, *171*, 347–352.
(17) Parker, C.; Rees, W. *Analyst* **1960**, *85*, 587–600.
(18) Cantor, C. R.; Schimmel, P. R. *Biophysical Chemistry. Part II: Techniques for the Study of Biological Structure and Function*; W. H. Freeman: San Francisco, CA, 1980.
(19) Young, M. E.; Carroad, P. A.; Bell, R. L. *Biotechnol. Bioeng.* **1980**, *22*, 947–955.
(20) Nkodo, A. E.; Garnier, J. M.; Tinland, B.; Ren, H.; Desruisseaux, C.; McCormick, L. C.; Drouin, G.; Slater, G. W. *Electrophoresis* **2001**, *22*, 2424–2432.